Impact of Climate Change on the Performance of Household-Scale Photovoltaic Systems

Nándor Bozsik [1]* , András Szeberényi [2] , Norbert Bozsik [3]

[1] *Donát Bánki Faculty of Mechanical and Safety Engineering, Óbuda University, 1081 Budapest, Hungary.*

[2] *Institute of Communications and Marketing, Budapest Metropolitan University, 1148 Budapest, Hungary.*

[3] *Institute of Agricultural and Food Economics, Hungarian University of Agriculture and Life Sciences, Hungary.*

Abstract

The objective of this article was to investigate the impacts of climate change on photovoltaic systems among renewable energies by the end of the 21st century. One hypothesis posited that due to decreased cloud cover as a result of changing climate, the geographical region under examination would receive more solar irradiation—usable by photovoltaic panels— which would in turn increase the annual electrical energy production of these systems. Another hypothesis suggested that the average temperature increase, associated with changing climate conditions, would detrimentally affect the efficiency of electricity production in photovoltaic systems. The study was based on the simulation of a household-scale photovoltaic model. This simulation calculated the system's performance on an hourly basis depending on inputs and summed these to produce an annual value. Input values were derived from climate scenario databases. These variables included global horizontal irradiance, direct horizontal irradiance, temperature, and wind speed. The output was the aforementioned quantity of annual electrical energy production. An analysis occurred between the annual average global horizontal irradiance and the annual average air temperature in relation to the quantities of annual electrical energy production. Pearson and partial correlation examinations among the variables demonstrated that unfavorable scenarios resulted in reduced efficiency of photovoltaic electrical energy production, primarily due to rising temperatures. Among other contributions, this article can support research into the active cooling of photovoltaic systems and the examination of their viability to mitigate efficiency losses caused by current and future temperature increases.

Keywords: Solar Panel; Warming; Efficiency; Climate Change; RCP Scenario.

1. Introduction

The three localities examined in the article are situated within the Carpathian Basin of Central Europe, on the territory of Hungary. Simulations were conducted for each locality with the same parameters over ten-year intervals from 2010 to 2100. For all three localities, temporal simulations were based on three distinct climate scenarios, resulting in nine time series for analysis. These results were analyzed based on the most significant variables for electrical energy production—global horizontal irradiance and air temperature. This focus is due to the performance of photovoltaic cells fundamentally depends on two quantities: the solar irradiance incident on the cells and the cells' temperature. The former has a positive impact, while the latter has a negative impact on photovoltaic energy production [1]. Naturally, more

---

factors are considered in the simulations. The incident solar radiation consists of both direct and diffuse radiation, with the latter further differentiated into atmospheric scattering and reflection from environmental surfaces such as soil, buildings, adjacent panel rows, etc. The temperature of photovoltaic cells fundamentally depends on the air temperature and the heat-generating effect of the current flowing within. The wind (speed, direction, humidity) and the parameters of heat-conducting elements (material, geometry) affect the dissipation of generated heat [2]. During fixed factors, a 38-degree tilt of southern-facing roofs was assumed, which conforms to Schuster's recommendations for maximizing annual yield at this latitude [3]. Additionally, the installation method partially influences the degree of heat dissipation mentioned earlier.

In the literature review, studies specifically examining the impact of climate change on photovoltaic electrical energy production in this geographic region are sparse or only tangentially addressed. Most available studies analyze technological scenarios that combine other renewable energies (such as wind power), like those by Campos et al. [4], or examine future targets and guidelines, as in Atsu et al. [5]. Some research investigates this theme from the perspective of future sustainability in energy diversification, especially regarding its economic and environmental aspects [6]. Noteworthy is the work by Baglivo et al., which studies changes in the photovoltaic (PV) systems' electricity supply as a consequence of climate change within a hypothetical mixed-energy community, analyzing the representative concentration pathways RCP4.5 and RCP8.5 in terms of photovoltaic energy production in two European cities, Berlin and Rome [7]. Relevant too is the study by Copiello and Grillenzoni, which employs a spatial autoregressive model to assess the geographic distribution of photovoltaic production capacity [8]. Oka et al.'s work also merits attention for considering future changes in energy production while taking into account the efficiency improvements in photovoltaic cells due to technological advancements [9]. There are also studies modeling changes in photovoltaic system energy production caused by climate change not based on climate scenarios but on mathematical probability forecasting [10] or machine learning [11–13], and others examining photovoltaic energy production in conjunction with other renewables in shaping future energy security [14]. This present study differs by performing correlation examinations between the primary input variables, the annual average solar irradiation and the annual average temperature, and the output variable, the quantity of annual electrical energy produced. It also conducts partial correlation analysis, considering each input variable as a control variable.

2. Material and Methods

2.1. The RCP

A notable deficiency observed in earlier climate change models pertained to their omission of critical factors, namely, the incorporation of climate mitigation measures and the adaptive capacity inherent to the Earth as a complex, dynamic system [15]. Consequently, in 2007, the Intergovernmental Panel on Climate Change (IPCC) issued a call to the global scientific community to embark on the development of novel climate change scenarios. This imperative led to the release of the AR5 report by the IPCC in 2014, wherein these new scenarios, known as Representative Concentration Pathways (RCPs), were unveiled. The RCP framework comprises an intricate database encompassing historical emissions, greenhouse gas concentrations, and alterations in land cover. Leveraging these datasets, the four distinctive RCP scenarios serve as vital inputs to climate models, enabling a more comprehensive exploration of potential future climate trajectories [16, 17].

2.2. The Radiative Forcing

Radiative forcing is an indicator of changes in the energy balance. This is caused by the presence of atmospheric "forcing" substances, which can be gas, dust, etc., that affect the global energy balance and contribute to climate change [18].

In Figure 1, the radiative forcing caused by global human activity is shown in high RCP8.5, medium-high RCP6, medium-low RCP4.5, and low RCP3-PD, also known as RCP2.6. In addition, there are two additional extensions: one that transitions the RCP6.0 level to RCP4.5 at 2250 (SCP6 to 4.5), and the other that transitions the RCP4.5 level to RCP3-PD (RCP2.6), which also leads to level 2250 (SCP45 to 3PD) [19–26].

Emission forcing levels refer to default median estimates. There is great uncertainty regarding current and future radiation forcing levels (Figure 1). Short-term fluctuations in the past (1800–2000) are due to cyclical solar forcing, assuming an 11-year solar cycle [19]. The RCP database was first published in May 2009. The RCP contains four harmonized and consolidated datasets covering emission pathways from the same base year (2000) to 2100. The database includes, among other things, emissions of greenhouse gases (GHGs). In addition to carbon dioxide, nitrous oxide, fluorinated gases, and short-lived greenhouse gases, radioactive and chemically active gases (black and organic carbon, methane, sulfur, nitrogen oxides, volatile organic compounds, carbon monoxide, and ammonia) also include Radiative forcing and greenhouse gas concentrations are given until 2100 in the case of RCPs but are extended to 2300, for example, in climate modeling. If available in archives, historical information is provided going back to 1850 [16].
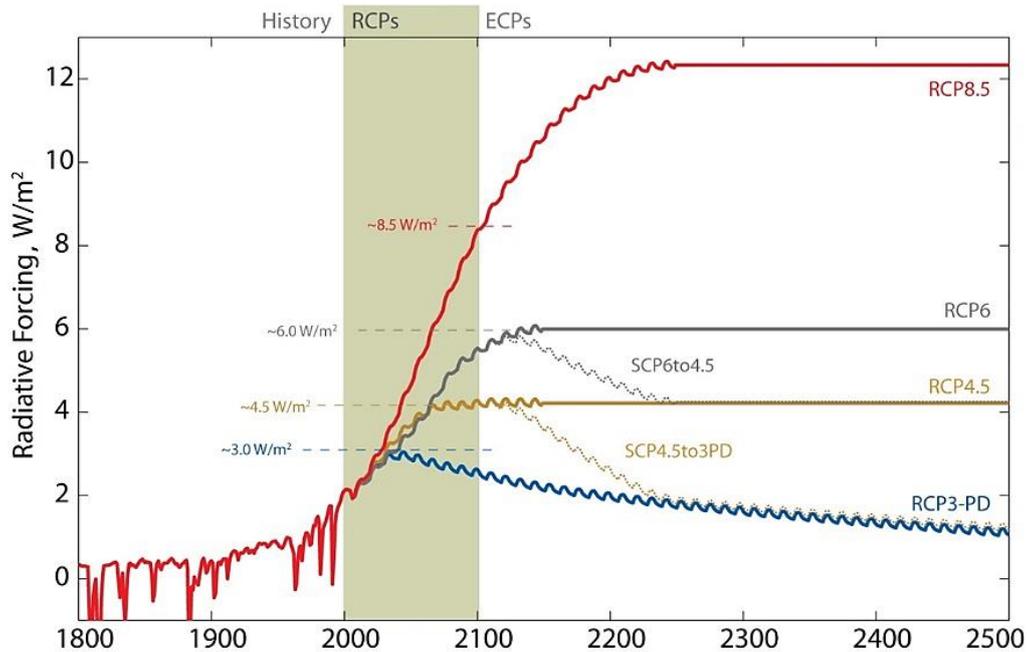
Figure 1. Radiative forcing trends based on the four RCP scenarios

2.3. Simulation

We simulate future production. For the simulation, we need to know the future development of environmental factors that are related to production. This is served by the aforementioned RCP scenarios, of which RCP2.6, RCP4.5, and RCP8.5 are used [19–23, 25].

The PVSyst program performing the simulation generates the input variables based on the RCP scenarios of the Meteonorm program. These are global horizontal radiation, diffuse horizontal radiation, air temperature, and wind speed. They are run per decade (2030–2100) at a resolution of the typical meteorological year (TMY) hours. The time-constant input values of the simulation program are the installation parameters. These are the type of panels, number of panels, tilt, and direction. The type of inverter is also determined, even though the comparative analysis refers to the direct current side power of the solar field (En =PDC), values that can be measured in front of the inverter. The output value of the inverter, the alternating current power (PAC), can serve as a basis for the subsequent analysis. Correlation analysis was made with the SPSS 25.0 program package (Figure 2).
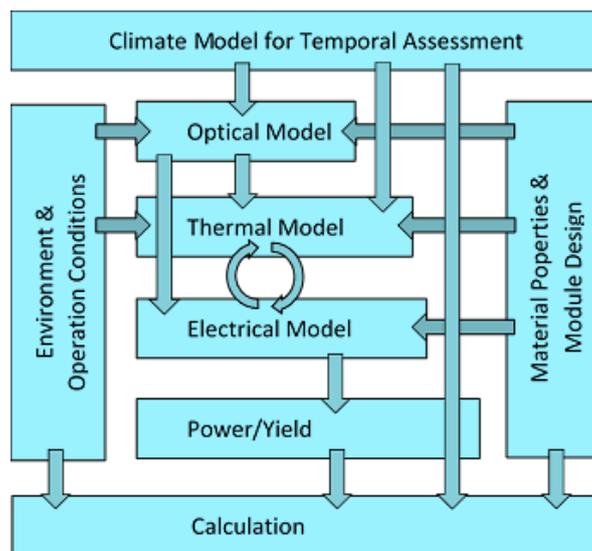
Figure 2. Flowchart of the simulation and calculation

2.4. Meteonorm Weather Database

The Meteonorm 8.0 database contains historical and contemporary data series. The periods 1981−1990 and 1996−2015 are available globally for solar radiation, and the periods 1961−1990 and 2000−2019 are available for all other

meteorological parameters. Meteonorm 8.0 provides access to historical time series of irradiance and temperature. The new archive contains hourly data from 2010. The model for the future was created based on current and RCP climate forecast trends. The RCP2.6, RCP4.5, and RCP 8.5 radiative forcing trend time series from 2020 to 2100 come from the RCP Database (Figure 3) [19–23, 25, 27–29].
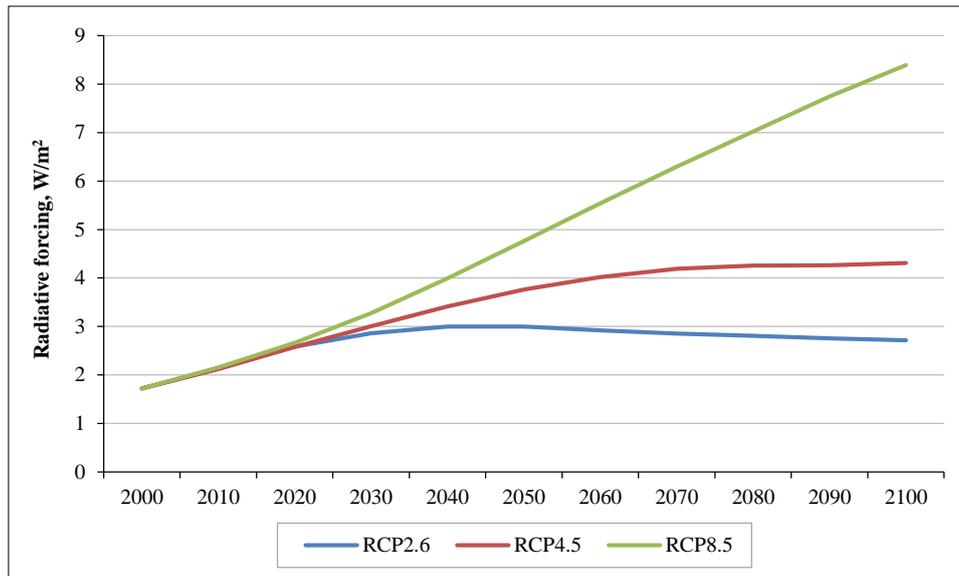
Figure 3. The RCP2.6, RCP4.5 and RCP8.5 scenarios

Meteonorm 8.0 generates the time series for the desired climate models from the above RCP trends, depending on the geographical location. For each RCP climate model, the program produces a typical meteorological year between 2020 and 2100 with a ten-year time interval resolution. That is, for example, between 2040 and 2050, it prepares the same data series for each year. The generated data series are stored in a file with the extension dot, which the PVSyst program can load to perform the simulations. These files contain, in hourly resolution, the global (Gh: global horizontal radiation, kWh/m^2) and diffuse (Dh: diffuse horizontal radiation, kWh/m^2) horizontal radiation, air temperature (Ta: air temperature, °C), and wind speed (WS: wind speed, m/s) data. Uncertainty of annual values: Gh = 2%, Ta = 0.3 °C; Gh trend/decade = 2.3%; Variability of Gh/year = 4.7%.

2.5. PVSyst Program

The evaluation of both present and prospective direct current (DC) and alternating current (AC) capabilities of the photovoltaic (PV) array has been meticulously conducted using the PVsyst version 7.2 software suite. This computational tool, originating from the esteemed University of Geneva, has been expressly designed for the detailed analysis, simulation, and schematic conception of PV installations. It incorporates an advanced three-dimensional modeling platform that rigorously accounts for the occlusion and shading dynamics imposed by proximate entities such as arboreal growths, edifices, and an assortment of structures (e.g., chimneys, antennas). The versatility of the software is demonstrated by its capability to assimilate meteorological datasets from an array of sources, including Meteonorm, NASA, and a spectrum of global research establishments. Moreover, it permits user-input data, amalgamated with discrete topographical and environmental parameters [29, 30].

Within the PVsyst package, the simulation encompasses a configuration of eighteen (2×9) LG 360 N1K-A6 monocrystalline silicon PV cells, coupled with a Fronius Symo 6.0-3-M inverter. Each PV module boasts an output of 360 watts, while the inverter's capacity is rated at 6 kilowatts. The deployment of the solar apparatus is executed on an autonomous structural framework, meticulously oriented due south (azimuth = 180 degrees) and pitched at an inclination of 38 degrees.

2.6. The Circuit and Mathematical Model

The physical mechanism underpinning the function of solar cells involves the interaction of incident photons with a semiconductor substrate composed primarily of silicon. These photons may be reflected, unimpededly transmitted, or assimilated by the cellular matrix. Absorbed photons impart their energy to the valence electrons within the semiconductor, precipitating the photovoltaic effect. This energetic transaction prompts an electron flux upon the establishment of an electrical circuit [31]. Conceptually, the solar cells can be envisaged as generators of current, as exemplified by the ideal cell block delineated in Figure 4. The currents emitted by these generators are then transmuted to the requisite voltage magnitude and waveform by employing a suitably selected electrical topology and interfaced

with the requisite current conversion apparatus (inverters) [32]. The PVsyst simulation used in this article uses the single-diode Perez-Ineichen model. The Hay model is also often used, which is mainly used when the diffuse irradiation data are not known precisely [33].
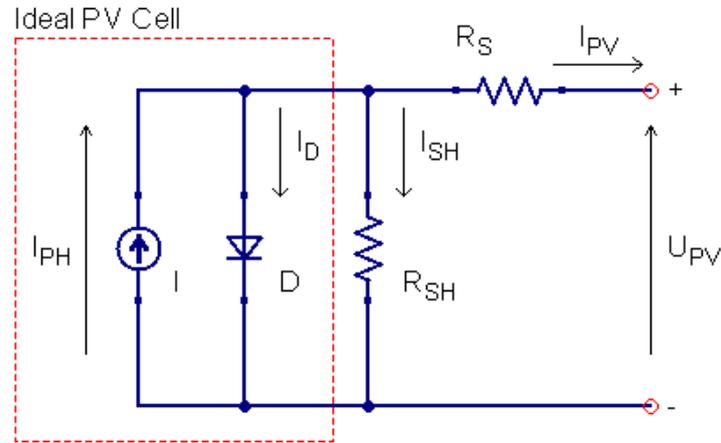
IPH: photocurrent, ID: diode current, ISH: parallel resistor, IS: series resistor, IPV: module current, UPV: module voltage

Figure 4. The one-diode solar cell model

In order to understand why it is not possible to simply "multiply" the radiation constraint curves of the RCP models and thus obtain the future yields, it is necessary to know the complexity of calculating the yield of solar panels.

The equation for the instantaneous power of the solar cell:

$$P(t) = U(t) \cdot I(t) \tag{1}$$

The current equation of a diode solar cell model:

$$I = I_{PH} - I_D - I_{SH} \tag{2}$$

where I is the module current, I_{PH} photocurrent, I_D diode current and I_{SH} is the current flowing through the parallel resistor is the shunt current (Figure 4):

$$I_{PH} = \left(\frac{G}{G_{ref}}\right) \cdot \left(I_{PHref} + mu_{ISC} \cdot (T_C - T_{Cref})\right) \tag{3}$$

where G and G_{ref} are the effective and reference radiation (W/m²), T_C and T_{Cref} are the effective and reference cell temperatures (°K), muisc is the temperature coefficient of the short-circuit current (A/°C). The value of G is calculated by the PVSyst program based on the global horizontal radiation (Gh) and diffuse horizontal radiation (Dh) from the Meteonorm database depending on the installation (inclination and azimuth angle) data, as well as the date and time. The T_C is calculated in Equation 7.

$$I_D = I_0 \left(e^{\frac{q \cdot (U + I \cdot R_S)}{N_{CS} \cdot Gamma \cdot k \cdot T_C}} - 1\right) \tag{4}$$

where I_0 is the short-circuit current of the diode, q is the charge of the electron (1.602·E-19 Coulomb), N_{CS} is the number of cells, Gamma is the quality factor of the diode a value between 1 and 2, k is Boltzmann's constant (1.381 E-23 J /°K).

$$I_0 = I_{0ref} \cdot \left(\frac{T_C}{T_{Cref}}\right)^3 \cdot e^{\left(\frac{q \cdot E_{Gap}}{Gamma \cdot k}\right) \cdot \left(\frac{1}{T_{Cref}} - \frac{1}{T_C}\right)} \tag{5}$$

where I_{0ref} is the short circuit reference current of the diode, E_{Gap} = Gap energy, which is 1.12 eV in the case of the Si crystal used in the study.

$$I_{SH} = \frac{U + I \cdot R_S}{R_{SH}} \tag{6}$$

where R_S is the series, R_{SH} shunt (parallel) resistance (Ohm).

$$T_c = T_a + G\frac{\alpha(1-eta_m)}{H_0 + H_1 \cdot WS} \qquad (7)$$

where eta_m is the efficiency of the PV module (0…1), *alfa* the absorption coefficient of the module (the default value of PVsyst is 0.9), H_0 is the constant heat transfer component (W/m^2), H_1 is the convective heat transfer component (W/m^2), WS: wind speed (m/s). Similarly to the determination of the G value, the Meteonorm database supplies the PVSyst program with the air temperature (T_a, in the program: T_a) and wind data (WS) needed to determine the cell temperature (T_c). The reference values of the solar panel are given based on the STC, where the manufacturer gives the parameters for irradiance of 1000 W/m^2, panel and ambient temperature of 25°C and atmospheric transparency of AM=1.5 (cloud factor) [33].

It is clear from the above that the current depends on many factors and these are included as non-linear terms in the equations. This is further complicated by the fact that the current-voltage value pairs form a series of curves depending on temperature (Figures 5 & 6). As the temperature increases, the short-circuit current increases and the no-load voltage decreases.
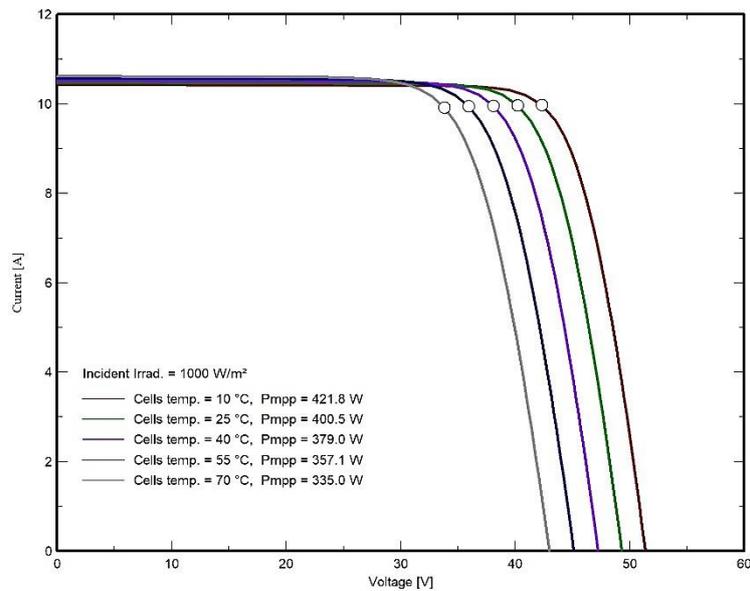
Figure 5. Temperature-dependent current-voltage curves
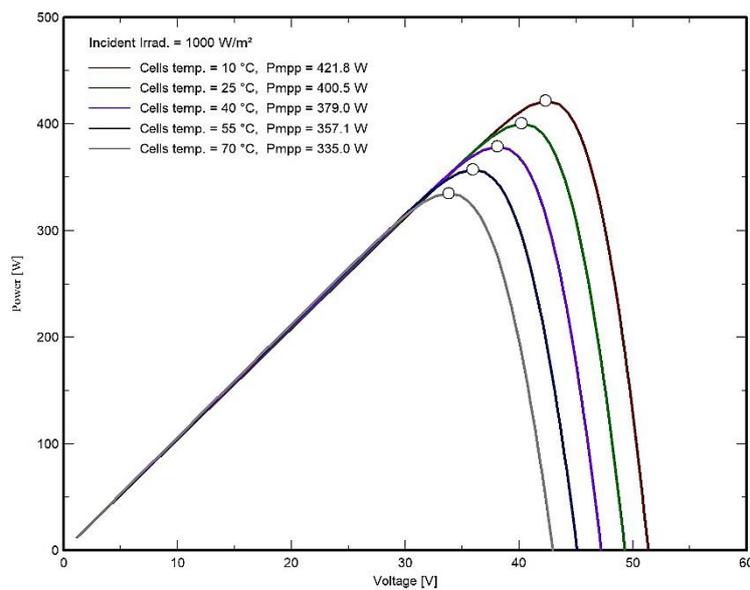
Figure 6 Temperature-dependent power-voltage curves

In other words, when calculating power, it must be taken into account that a given current value has different voltages at different temperatures [34].

Calculation of the annual yield:

$$E = \int_0^t U(t)I(t)dt \tag{8}$$

where t is the time, here is the length of a year.

In the course of the simulation, the objective is not to integrate the current-voltage product over a single year; rather, data points are cumulatively analyzed on an hourly, quarter-hourly, or decaminute basis throughout the annual cycle to yield the annual energy output (En). The conversion calculations from DC to AC power are complexified by the consideration of not only the energy utilized by the interposed inverter but also by the necessity to account for the non-ideal operational envelope of the inverter. The latter does not perpetually operate at the maximum power point (MPP) — the operational state where the product of current and voltage reaches its apex, thereby engendering further systemic losses.

2.7. SPSS 25.0 Program

The interrelations between the input and output variables were examined utilizing the IBM SPSS 25.0 statistical software to construct a correlation matrix and conduct partial correlation tests. Within this matrix, the coefficients represent the magnitude of linear associations between variables. Significance levels at both one and five percent are denoted, providing a clear indication of statistical robustness. Partial correlation analysis, controlling for third variables, allows for the assessment of direct relationships between two variables, independent of the control variable's influence. This analytical technique is essential in discerning whether the observed correlations persist when the effects of the control variable are statistically removed [35].

3. Results

In this section, the simulation outcomes for RCP2.6, RCP4.5, and RCP8.5 have been presented in tables. These tables detail essential climatological and photovoltaic output parameters, including global horizontal irradiance (Ghi), ambient air temperature (Ta), and the annual yield of direct current power (En). It should be noted that while diffuse horizontal radiation and mean wind speed data are not displayed within these tables, such variables were incorporated into the simulation algorithms.

3.1. The Climate of the Budapest-Pestszentlőrinc Area

The meteorological dataset for Budapest originates from the Pestszentlőrinc station. This station's geographical coordinates are 47.4°N latitude and 19.2°E longitude, situated at an elevation of 140 meters above sea level. An analysis of the Budapest-Pestszentlőrinc climate data indicates January as the most frigid month, with July registering as the most temperate. An average annual thermal amplitude of 22.0 °C is observed, coupled with a mean annual precipitation total of 525 mm. Seasonal variation in solar irradiance is pronounced, with peak values in June and July and nadir in the November to January interval (Table 1) [36].

Table 1. Budapest-Pestszentlőrinc time series

	Annual	2010	2020	2030	2040	2050	2060	2070	2080	2090	2100
RCP2.6	Gh, kWh/m^2	1223	1252	1281	1292	1299	1303	1307	1307	1307	1310
	Ta, °C	11.8	12.2	12.7	12.9	13.2	13.3	13.2	13.2	13.1	13.1
	En, kWh	7962	8158	8345	8425	8527	8541	8546	8588	8569	8563
RCP4.5	Gh, kWh/m^2	1223	1241	1259	1267	1270	1270,65	1281	1288	1292	1296
	Ta, °C	11.8	12.2	12.6	13.0	13.4	13.9	14.0	14.3	14.5	14.8
	En, kWh	7962	8063	8163	8266	8248	8365	8229	8313	8269	8299
RCP8.5	Gh, kWh/m^2	1223	1241	1259	1270	1281	1288	1292	1296	1303	1307
	Ta, °C	11.8	12.3	12.9	13.5	14.1	14.9	15.5	16.2	16.9	17.6
	En, kWh	7962	8138	8171	8314	8293	8336	8388	8354	8416	8397

3.2. The Climate of the Szeged Region

The meteorological data for Szeged is derived from a station located on the periphery of the city. The geographical positioning of this station is recorded at 46.3°N latitude and 20.1°E longitude, at an altitude of 82 meters. Temperature recordings from this station indicate January as the coldest month, while July is identified as the warmest, marginally surpassing August by a tenth of a degree Celsius. The mean annual temperature range is calculated at 21.7 °C. Annual precipitation averages at 534 mm, with January being the driest and June the most humid, receiving nearly thrice the

precipitation of the driest month. A similar pattern of global radiation is observed here, with a peak in July and the lowest readings in the December to January timeframe (Table 2) [36].

Table 2. Time series of Szeged

	Annual	2010	2020	2030	2040	2050	2060	2070	2080	2090	2100
RCP2.6	Gh, kWh/m²	1237	1267	1299	1307	1321	1325	1325	1325	1325	1325
	Ta, °C	11.7	12.3	12.6	12.9	13.1	13.3	13.2	13.2	13.1	13.1
	En, kWh	7968	8125	8404	8475	8560	8625	8595	8608	8562	8576
RCP4.5	Gh, kWh/m²	1237	1256	1278	1281	1288	1292	1299	1303	1307	1310
	Ta, °C	11.7	12.2	12.7	13.1	13.4	13.7	14.0	14.2	14.5	14.8
	En, kWh	7968	8097	8221	8203	8221	8259	8353	8342	8398	8323
RCP8.5	Gh, kWh/m²	1237	1256	1278	1288	1299	1307	1310	1318	1321	1329
	Ta, °C	11.7	12.4	12.8	13.5	14.1	14.8	15.6	16.2	16.9	17.6
	En, kWh	7968	8105	8254	8285	8316	8422	8469	8526	8466	8500

3.3. The Climate of the Szombathely Area

The meteorological dataset for Szombathely is obtained from the local station, positioned at 47.3°N latitude, 16.6°E longitude, and an elevation of 224 meters. An examination of Szombathely's temperature data reveals January as the month with the lowest average temperatures, while July registers as the warmest. The city experiences an average annual temperature fluctuation of 22.6 °C. The mean annual precipitation is 614 mm, with a notable seasonal disparity: a wetter summer semester juxtaposed against a drier winter semester. January is marked as the driest month, whereas the summer months collectively receive approximately threefold the precipitation of January. Solar irradiance in Szombathely attains its zenith in June and July, with its nadir occurring from November to January (Table 3) [36].

Table 3. Szombathely time series

	annual	2010	2020	2030	2040	2050	2060	2070	2080	2090	2100
RCP2.6	Gh, kWh/m²	1186	1212	1241	1248	1256	1259	1259	1259	1256	1256
	Ta, °C	10.8	11.2	11.6	11.8	12.0	12.1	12.0	12.0	11.9	11.9
	En, kWh	7769	7976	8076	8181	8232	8187	8220	8191	8163	8149
RCP4.5	Gh, kWh/m²	1186	1205	1219	1226	1234	1241	1241	1245	1248	1252
	Ta, °C	10.8	11.2	11.6	11.9	12.4	12.7	12.9	13.1	13.5	13.6
	En, kWh	7769	7790	7911	7948	7952	8015	8025	8001	8005	8035
RCP8.5	Gh, kWh/m²	1186	1205	1219	1230	1241	1248	1252	1256	1267	1270
	Ta, °C	10.8	11.4	11.8	12.4	13.0	13.7	14.4	15.2	15.9	16.5
	En, kWh	7769	7834	7942	7939	8017	8102	8029	8124	8115	8155

Explanation to Figures 7 to 15: ΔGh represents the percentage deviation of the annual average global horizontal irradiation relative to the base year of 2010; ΔTa denotes the change in the annual average air temperature compared to the base year of 2010; ΔEn indicates the percentage change in the electrical energy production of the PV system compared to the base year of 2010. The RCP2.6, RCP4.5, and RCP8.5 correspond to the progression of the respective RCP scenarios.

3.4. Graphical Evaluation for Budapest, Szeged, and Szombathely based on the base Year of 2010

For the Budapest climate projections, the RCP2.6, RCP4.5, and RCP8.5 forecast alterations in global horizontal irradiance (GHI) by 6.3%, 3.9%, and 4.8%, respectively, and shifts in average air temperature by 1.4°C, 1.6°C, and 2.3°C, correspondingly. In addition, direct current (DC) power output is projected to vary by 7.1%, 3.6%, and 4.2% by the midpoint of the century. By the century's conclusion, GHI is anticipated to adjust by 7.2%, 6.0%, and 6.9%, while average air temperatures are expected to alter by 1.3°C, 3.0°C, and 5.8°C. Concurrently, DC power output is projected to register changes of 7.6%, 4.2%, and 5.5% (Figures 7 to 9).
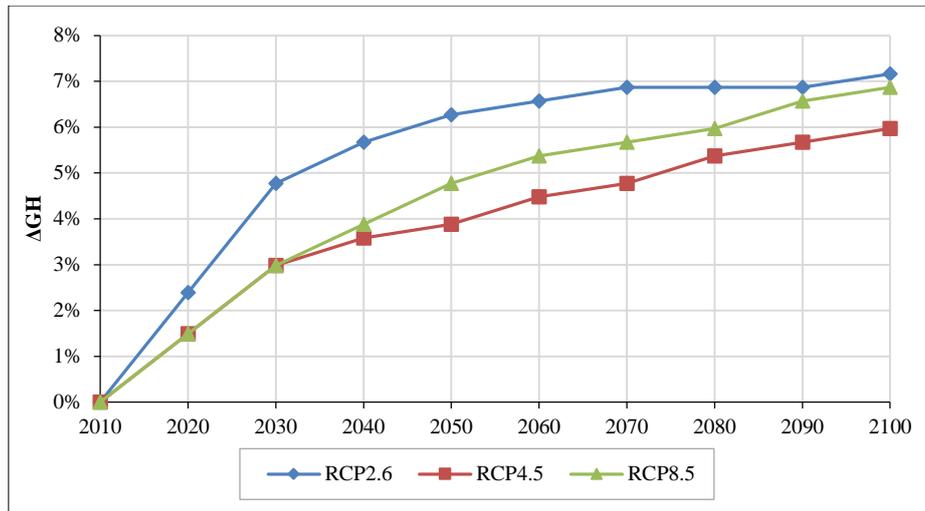
Figure 7. Budapest global horizontal radiation, base year: 2010
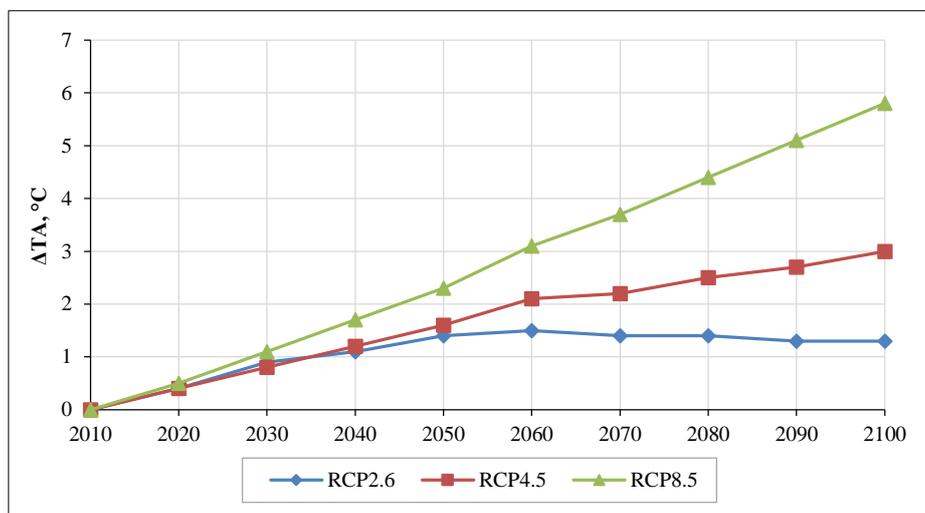
Figure 8. Budapest annual mean temperature, base year: 2010
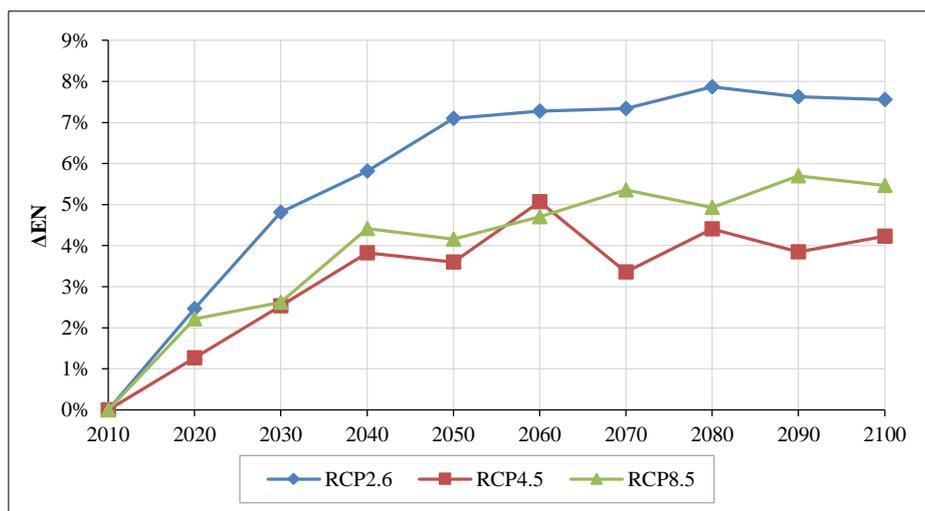
Figure 9. Budapest change in DC electricity production, base year: 2010

In the case of Szeged, under the RCP2.6, RCP4.5, and RCP8.5 scenarios, there are respective projections of 6.8%, 4.1%, and 5.0% for GHI changes, and 1.4°C, 1.7°C, and 2.4°C for average air temperature changes by mid-century. By the century's end, GHI is forecasted to alter by 7.1%, 5.9%, and 7.4%, while average air temperature is projected to change by 1.4°C, 3.1°C, and 5.9°C. Corresponding shifts in DC power output are anticipated at 7.6%, 4.5%, and 6.7% (Figure 10-12).
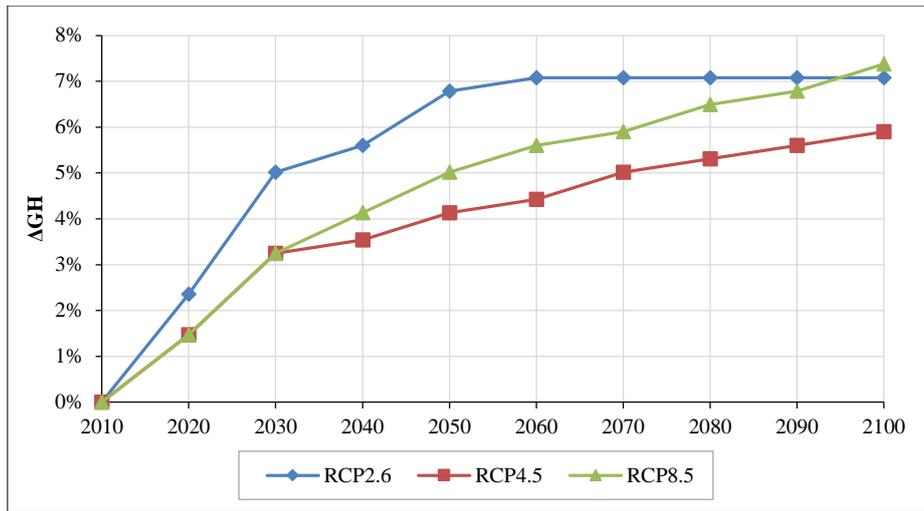
Figure 10. Szeged global horizontal radiation, base year: 2010
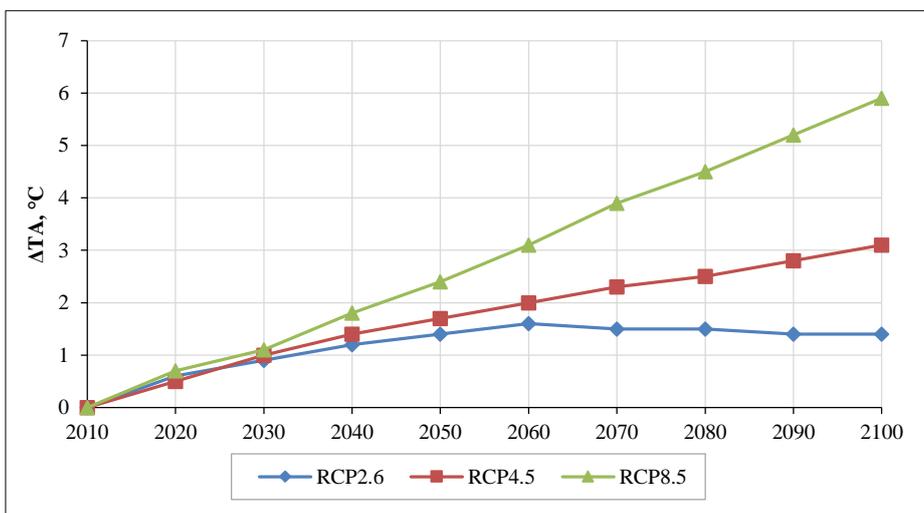
Figure 11. Szeged annual mean temperature, base year: 2010
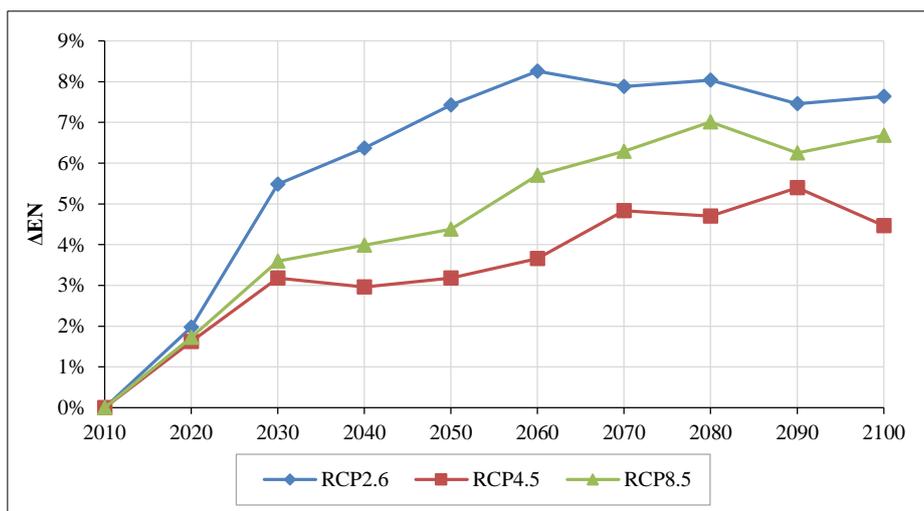
Figure 12. Szeged change in DC electricity production, base year: 2010

In the case of Szombathely, scenario analyses for RCP2.6, RCP4.5, and RCP8.5 suggest respective changes in GHI by 5.9%, 4.0%, and 4.6%, and in average air temperature by 1.2°C, 1.6°C, and 2.2°C by the mid-21st century. Toward the end of the century, projections indicate adjustments in GHI by 5.9%, 5.5%, and 7.1%, and in average air temperature by 1.1°C, 2.8°C, and 5.7°C. The predicted shifts in DC power output are 4.9%, 3.4%, and 5.0% (Figure 13 to 15).
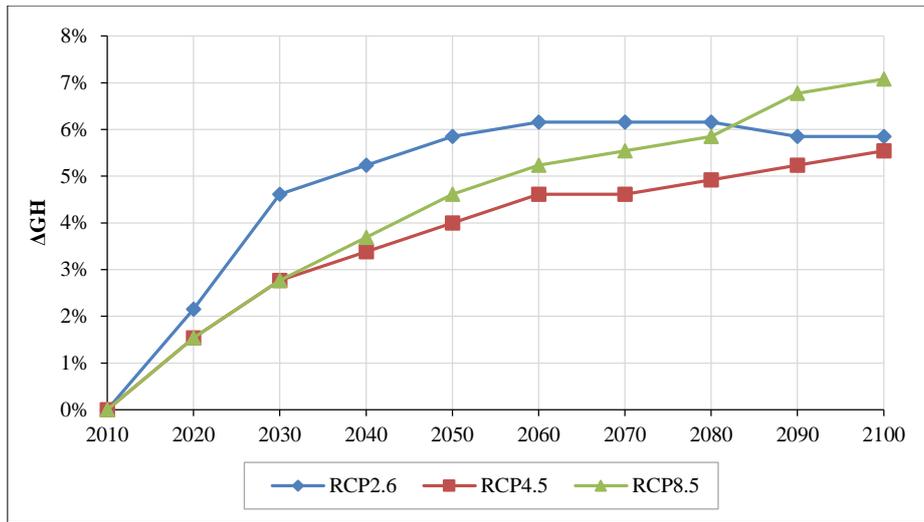
Figure 13. Szombathely global horizontal radiation, base year: 2010
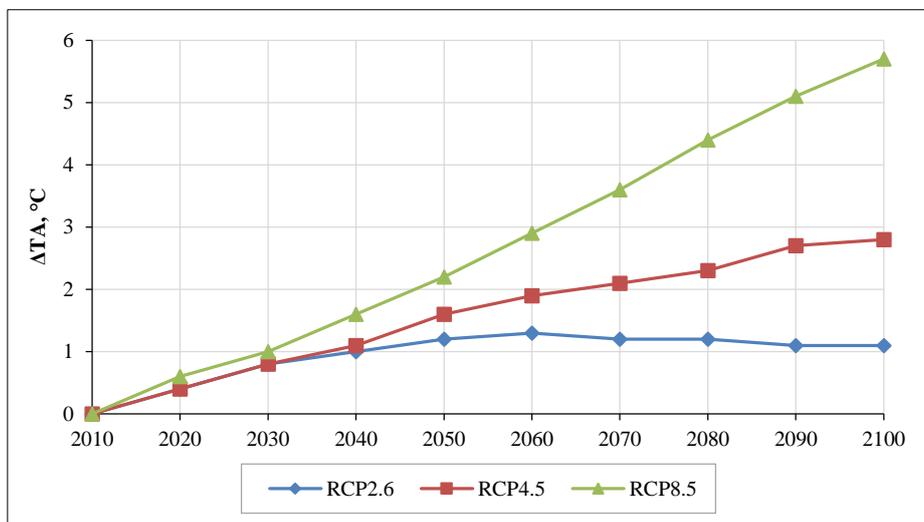
Figure 14. Szombathely annual mean temperature, base year: 2010
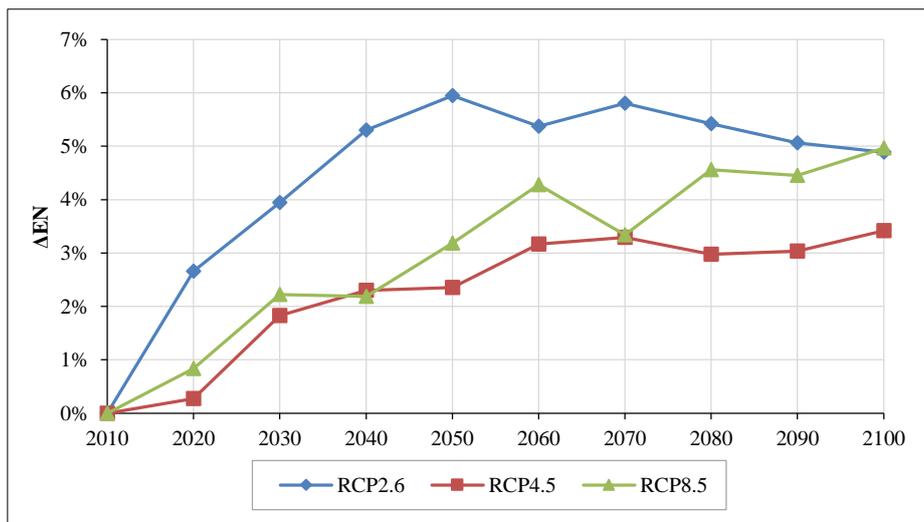
Figure 15. Szombathely change in DC electricity production, base year: 2010

It is pertinent to underscore that prior to integration into the power grid, the DC output from photovoltaic arrays incurs an approximate decrement of 4–4.5 percent. This attenuation is attributed to the conversion processes from DC to DC and DC to AC, primarily facilitated by inverters, and is compounded by losses inherent to cabling.

3.5. Correlation Study

The correlation analysis was undertaken to elucidate the interdependencies among global radiation, ambient air temperature, and photovoltaic module efficacy (Table 4). The underlying assumption posits that due to the semiconductor properties inherent in solar cells, elevated temperatures detrimentally impact their operational efficiency.

Table 4. Correlation matrix between global radiation, temperature and power

			Gh_2.6	Ta_2.6		Gh_4.5	Ta_4.5		Gh_8.5	Ta_8.5
Budapest	corr.	Ta_2.6	0.980		Ta_4.5	0.974		Ta_8.5	0.947	
	sig.		0.000			0.000			0.000	
	corr.	En_2.6	0.995	0.986	En_4.5	0.902	0.847	En_8.5	0.970	0.878
	sig.		0.000	0.000		0.000	0.002		0.000	0.001
Szeged	corr.	Ta_2.6	0.987		Ta_4.5	0.977		Ta_8.5	0.947	
	sig.		0.000			0.000			0.000	
	corr.	En_2.6	0.995	0.986	En_4.5	0.971	0.936	En_8.5	0.983	0.919
	sig.		0.000	0.000		0.000	0.000		0.000	0.000
Szombathely	corr.	Ta_2.6	0.992		Ta_4.5	0.968		Ta_8.5	0.955	
	sig.		0.000			0.000			0.000	
	corr.	En_2.6	0.975	0.975	En_4.5	0.971	0.925	En_8.5	0.974	0.929
	sig.		0.000	0.000		0.000	0.000		0.000	0.000

In all three scenarios under consideration, a pronounced correlation among the studied variables is observed. This phenomenon can be primarily attributed to the direct relationship wherein elevated levels of global horizontal radiation (GHR) engender increased temperature indices. Consequently, the strong correlation between average temperature and system performance might lead to an erroneous inference that higher average temperatures are a causative agent for enhanced performance. To disentangle these variables, it is imperative to employ a partial correlation analysis (Table 5), wherein GHR is held constant in one instance and average air temperature in another, serving as the background variables for the analysis.

Table 5. Partial correlations

	Cont. Var.	Var. 1	Var. 2	Corr.	Sig.
Budapest	Ta_2.6	Gh_2.6	En_2.6	0.869	0.002
	Gh_2.6	Ta_2.6	En_2.6	0.555	0.121
	Ta_4.5	Gh_4.5	En_4.5	0.643	0.062
	Gh_4.5	Ta_4.5	En_4.5	-0.329	0.387
	Ta_8.5	Gh_8.5	En_8.5	0.898	0.001
	Gh_8.5	Ta_8.5	En_8.5	-0.505	0.166
Szeged	Ta_2.6	Gh_2.6	En_2.6	0.810	0.008
	Gh_2.6	Ta_2.6	En_2.6	0.280	0.466
	Ta_4.5	Gh_4.5	En_4.5	0.751	0.020
	Gh_4.5	Ta_4.5	En_4.5	-0.237	0.539
	Ta_8.5	Gh_8.5	En_8.5	0.887	0.001
	Gh_8.5	Ta_8.5	En_8.5	-0.190	0.624
Szombathely	Ta_2.6	Gh_2.6	En_2.6	0.287	0.453
	Gh_2.6	Ta_2.6	En_2.6	0.287	0.455
	Ta_4.5	Gh_4.5	En_4.5	0.791	0.011
	Gh_4.5	Ta_4.5	En_4.5	-0.240	0.533
	Ta_8.5	Gh_8.5	En_8.5	0.796	0.010
	Gh_8.5	Ta_8.5	En_8.5	-0.034	0.932

When examining the partial correlations with temperature as the control variable, a persistently robust correlation between GHR and power output is generally maintained. However, the Szombathely RCP2.6 scenario constitutes a notable exception to this pattern. Further, when assessing the relationship between temperature and power output with

GHR as the control variable, the partial correlation ceases to exhibit significant levels of correlation. This decrement is even more pronounced under the RCP4.5 and RCP8.5 scenarios, where the correlation values invert, becoming negative. Such a reversal suggests that, within the context of these latter scenarios, the escalation in temperature is likely to be deleterious to the operational efficiency of photovoltaic panel systems, thereby mitigating power production efficacy.

4. Conclusions

Based on the correlation between input data and the output of the simulation, the efficiency of the photovoltaic system exhibits significant variations. This is markedly dependent on whether an optimistic or pessimistic scenario is considered with respect to climate change. In the case of the optimistic Representative Concentration Pathway (RCP) 2.6 scenario, the performance of the photovoltaic system increases almost linearly due to the rise in global horizontal irradiation caused by increasing radiative forcing and a slight average increase in air temperature. However, this linearity is not present in the less optimistic or pessimistic RCP 4.5 and RCP 8.5 scenarios. The value of the partial correlation, which uses global horizontal irradiation as a control variable, is negative. This indicates a decrease in system efficiency concurrent with an annual average increase in air temperature.

One limitation of the study's reliability is the input values provided by the Meteonorm database, which are derived from monthly climate data values. The database produces hourly resolution input values for the simulation based on given variances and expected values. A deficiency is the lack of intra-annual comparison between the summer and winter seasons, as it can be assumed that the efficiency decrease due to temperature change is more likely to occur during the summer period. Furthermore, a significant portion of the annual solar energy production in this region falls between mid-April and mid-October. Another limitation of the study is that it examines only monocrystalline solar cells; there is a need for a comparison with polycrystalline and thin-film technology solar cells. Monocrystalline solar cells are the most efficient, while thin-film technology cells, due to their internal properties, are more resistant to high temperatures. Polycrystalline solar cell technology is advantageous due to the availability of resources [12].

Despite growing interest, however, few studies have directly examined the impact of climate change on photovoltaic energy production as opposed to other renewable sources such as hydro or wind energy [37]. The results of the few studies that do exist on this topic show significant discrepancies. Gaetani et al. found increased PV potential in Southern and Western Europe, while Northern and Eastern Europe are expected to decline by the middle and end of the century based on the IPCC (Intergovernmental Panel on Climate Change's) emissions scenarios [38]. According to Dutta et al., the expected changes in solar radiation support a general increase in PV potential in Europe in the near future. The predicted distant decline in photovoltaic potential, even in the worst emission scenario (RCP8.5), is confined to the winter season and to northern countries in Europe [39]. Crook et al.'s calculations suggest that PV efficiency is likely to increase by a few percent in Europe between 2010 and 2080 [40]. Gernet et al., considering the RCP6.0 climate scenario, estimate an increase in solar energy yield efficiency of 5–10% in the Central European region between 2070 and 2100, which is consistent with the findings of the present study. The RCP6.0 climate scenario defines a trajectory between the RCP4.5 and RCP8.5 climate scenarios [41].

5. Declarations

5.1. Author Contributions

Conceptualization, Na.B., A.S., and N.B.; methodology, Na.B. and N.B.; software, Na.B. and N.B.; validation, Na.B., A.S., and N.B.; formal analysis, Na.B. and N.B.; investigation, Na.B. and N.B.; resources, Na.B, A.S., and N.B.; data curation, Na.B.; writing—original draft preparation, Na.B. and N.B.; writing—review and editing, A.S.; visualization, Na.B. and N.B.; supervision, A.S.; project administration, A.S.; funding acquisition, A.S. All authors have read and agreed to the published version of the manuscript.

5.2. Data Availability Statement

The data presented in this study are available in the article.

5.3. Funding

The authors received no financial support for the research, authorship, and/or publication of this article.

5.4. Institutional Review Board Statement

Not applicable.

5.5. Informed Consent Statement

Not applicable.

5.6. Declaration of Competing Interest

The authors declare that they have no known competing financial interests or personal relationships that could have appeared to influence the work reported in this paper.

6. References

[1] Simioni, T., & Schaeffer, R. (2019). Georeferenced operating-efficiency solar potential maps with local weather conditions – An application to Brazil. Solar Energy, 184, 345–355. doi:10.1016/j.solener.2019.04.006.

[2] Singh, P., & Ravindra, N. M. (2012). Temperature dependence of solar cell performance - An analysis. Solar Energy Materials and Solar Cells, 101, 36–45. doi:10.1016/j.solmat.2012.02.019.

[3] Schuster, C. S. (2020). The quest for the optimum angular-tilt of terrestrial solar panels or their angle-resolved annual insolation. Renewable Energy, 152, 1186–1191. doi:10.1016/j.renene.2020.01.076.

[4] Campos, J., Csontos, C., & Munkácsy, B. (2023). Electricity scenarios for Hungary: Possible role of wind and solar resources in the energy transition. Energy, 278. doi:10.1016/j.energy.2023.127971.

[5] Atsu, D., Seres, I., & Farkas, I. (2021). The state of solar PV and performance analysis of different PV technologies grid-connected installations in Hungary. Renewable and Sustainable Energy Reviews, 141. doi:10.1016/j.rser.2021.110808.

[6] Madaleno, M., Ahmed, Z., Doğan, B., Javeed, S., & Vasa, L. (2023). The aptness of import-led growth hypothesis for sustainable development in South Asia: Do energy utilization and natural resources matter? Resources Policy, 86. doi:10.1016/j.resourpol.2023.104262.

[7] Baglivo, C., Congedo, P. M., & Mazzeo, D. (2023). Scenarios for urban resilience—perspective on climate change resilience at the end of the 21st century of a photovoltaic-powered mixed-use energy community in two European capitals. Adapting the Built Environment for Climate Change: Design Principles for Climate Emergencies, Woodhead Publishing, 37–52. doi:10.1016/B978-0-323-95336-8.00012-3.

[8] Copiello, S., & Grillenzoni, C. (2017). Solar Photovoltaic Energy and Its Spatial Dependence. Energy Procedia, 141, 86–90. doi:10.1016/j.egypro.2017.11.017.

[9] Oka, K., Mizutani, W., & Ashina, S. (2020). Climate change impacts on potential solar energy production: A study case in Fukushima, Japan. Renewable Energy, 153, 249–260. doi:10.1016/j.renene.2020.01.126.

[10] Abdulai, D., Gyamfi, S., Diawuo, F. A., & Acheampong, P. (2023). Data analytics for prediction of solar PV power generation and system performance: A real case of Bui Solar Generating Station, Ghana. Scientific African, 21. doi:10.1016/j.sciaf.2023.e01894.

[11] Ghimire, S., Deo, R. C., Casillas-Pérez, D., & Salcedo-Sanz, S. (2022). Boosting solar radiation predictions with global climate models, observational predictors and hybrid deep-machine learning algorithms. Applied Energy, 316. doi:10.1016/j.apenergy.2022.119063.

[12] Nwokolo, S. C., Obiwulu, A. U., & Ogbulezie, J. C. (2023). Machine learning and analytical model hybridization to assess the impact of climate change on solar PV energy production. Physics and Chemistry of the Earth, 130. doi:10.1016/j.pce.2023.103389.

[13] Chukwujindu Nwokolo, S., Ogbulezie, J. C., & Umunnakwe Obiwulu, A. (2022). Impacts of climate change and meteo-solar parameters on photosynthetically active radiation prediction using hybrid machine learning with Physics-based models. Advances in Space Research, 70(11), 3614–3637. doi:10.1016/j.asr.2022.08.010.

[14] Svazas, A.M., Navickas, V., Paskevicius, R., Bilan, Y. & Vasa, L. (2023). Renewable Energy versus Energy Security: The Impact of In-Novation on the Economy. Rynek Energii 164(1), 60-71.

[15] Nakicenovic, N., Alcamo, J., Grubler, A., Riahi, K., Roehrl, R.A., Rogner, H.-H. , & Victor, N. (2000). Special Report on Emissions Scenarios (SRES), A Special Report of Working Group III of the Intergovernmental Panel on Climate Change. Cambridge University Press, Cambridge, United Kingdom.

[16] Riahi, K., & Krey, V. (2023). Representative Concentration Pathways Database (RCP). International Institute for Applied Systems Analysis (IIASA), Laxenburg, Austria. Available online: https://iiasa.ac.at/models-tools-data/rcp (accessed on June 2023).

[17] Mester, M., A. (2015). Comparison of new RCP emission scenarios for estimating global climate change. ELTE, Budapest, Hungary. Available online: https://nimbus.elte.hu/tanszek/docs/BSc/2015/MesterMateAttila_2015.pdf (accessed on May 2023).

[18] He, T., Wang, D., & Qu, Y. (2017). Land surface albedo. Comprehensive Remote Sensing, 1–9, 140–162. doi:10.1016/B978-0-12-409548-9.10370-7.

[19] Meinshausen, M., Smith, S. J., Calvin, K., Daniel, J. S., Kainuma, M. L. T., Lamarque, J., Matsumoto, K., Montzka, S. A., Raper, S. C. B., Riahi, K., Thomson, A., Velders, G. J. M., & van Vuuren, D. P. P. (2011). The RCP greenhouse gas concentrations and their extensions from 1765 to 2300. Climatic Change, 109(1), 213–241. doi:10.1007/s10584-011-0156-z.

[20] Van Vuuren, D. P., Den Elzen, M. G. J., Lucas, P. L., Eickhout, B., Strengers, B. J., Van Ruijven, B., Wonink, S., & Van Houdt, R. (2007). Stabilizing greenhouse gas concentrations at low levels: An assessment of reduction strategies and costs. Climatic Change, 81(2), 119–159. doi:10.1007/s10584-006-9172-9.

[21] Clarke, L., Edmonds, J., Jacoby, H., Pitcher, H., Reilly, J. & Richels, R. (2007). Scenarios of Greenhouse Gas Emissions and Atmopheric Concentrations. Sub-report 2.1A of Synthesis and Assessment Product 2.1 by the U.S. Climate Change Science Program and the Subcommittee on Global Change Research. Department of Energy, Office of Biological & Environmental Research, 154, Washington, United States.

[22] Smith, S. J., & Wigley, T. M. L. (2006). Multi-gas forcing stabilization with minicam. Energy Journal, 27, 373–391. doi:10.5547/issn0195-6574-ej-volsi2006-nosi3-19.

[23] Wise, M., Calvin, K., Thomson, A., Clarke, L., Bond-Lamberty, B., Sands, R., Smith, S. J., Janetos, A., & Edmonds, J. (2009). Implications of limiting CO_2 concentrations for land use and energy. Science, 324(5931), 1183–1186. doi:10.1126/science.1168475.

[24] Fujino, J., Nair, R., Kainuma, M., Masui, T., & Matsuoka, Y. (2006). Multi-gas mitigation analysis on stabilization scenarios using aim global model. Energy Journal, 27, 343–353. doi:10.5547/issn0195-6574-ej-volsi2006-nosi3-17.

[25] Riahi, K., Grübler, A., & Nakicenovic, N. (2007). Scenarios of long-term socio-economic and environmental development under climate stabilization. Technological Forecasting and Social Change, 74(7), 887–935. doi:10.1016/j.techfore.2006.05.026.

[26] Márton, Z., Szabó, B., Vad, C. F., Pálffy, K., & Horváth, Z. (2023). Environmental changes associated with drying climate are expected to affect functional groups of pro-and microeukaryotes differently in temporary saline waters. Scientific Reports, 13(1), 3243. doi:10.1186/s12302-023-00745-0.

[27] Meteonorm (2023). Meteonorm offers unique access to the Global Energy Balance Archive Data, Meteonorm Data sources. Available online: https://meteonorm.com/en/meteonorm-features (accessed on June 2023).

[28] IIASA. (2009). RCP Database Version 2.0.5. International Institute for Applied Systems Analysis. Laxenburg, Austria. Available online: https://tntcat.iiasa.ac.at/RcpDb/dsd?Action=htmlpage&page=compare (accessed on June 2023).

[29] Li, J., Li, Y., Zhu, B., & Ma, X. (2021). Analysis of hydrogen production capacity of off-grid photovoltaic system based on PVsyst software simulation. Journal of Physics: Conference Series, 2076(1), 12005. doi:10.1088/1742-6596/2076/1/012005.

[30] Bhuvaneswari, B., D, S., & Memala, W. A. (2022). Performance Analysis of Stand-Alone Photovoltaic System Using PVsyst. ECS Transactions, 107(1), 11533–11541. doi:10.1149/10701.11533ecst.

[31] Ready, J. F. (1997). Care and Maintenance of Lasers. Industrial Applications of Lasers, 193–214. doi:10.1016/b978-012583961-7/50008-9.

[32] Markvart, T., & Castañer, L. (2018). Principles of solar cell operation. McEvoy's Handbook of Photovoltaics: Fundamentals and Applications, 3–28. doi:10.1016/B978-0-12-809921-6.00001-X.

[33] Perez, R., Ineichen, P., Seals, R., Michalsky, J., & Stewart, R. (1990). Modeling daylight availability and irradiance components from direct and global irradiance. Solar Energy, 44(5), 271–289. doi:10.1016/0038-092X(90)90055-H.

[34] Seapan, M., Hishikawa, Y., Yoshita, M., & Okajima, K. (2020). Temperature and irradiance dependences of the current and voltage at maximum power of crystalline silicon PV devices. Solar Energy, 204, 459–465. doi:10.1016/j.solener.2020.05.019.

[35] Meloun, M., & Militký, J. Correlation. Statistical Data Analysis, 631–666. doi:10.1533/9780857097200.631.

[36] OMSZ (2023). The Hungarian Meteorological Service (OMSZ). OMSZ Informatics and Methodology Department, Budapest, Hungary. Available online: https://www.met.hu/en/eghajlat/magyarorszag_eghajlata/ (accessed on June 2023).

[37] Schaeffer, R., Szklo, A. S., Pereira de Lucena, A. F., Moreira Cesar Borba, B. S., Pupo Nogueira, L. P., Fleming, F. P., Troccoli, A., Harrison, M., & Boulahya, M. S. (2012). Energy sector vulnerability to climate change: A review. Energy, 38(1), 1–12. doi:10.1016/j.energy.2011.11.056.

[38] Gaetani, M., Huld, T., Vignati, E., Monforti-Ferrario, F., Dosio, A., & Raes, F. (2014). The near future availability of photovoltaic energy in Europe and Africa in climate-aerosol modeling experiments. Renewable and Sustainable Energy Reviews, 38, 706–716. doi:10.1016/j.rser.2014.07.041.

[39] Dutta, R., Chanda, K., & Maity, R. (2022). Future of solar energy potential in a changing climate across the world: A CMIP6 multi-model ensemble analysis. Renewable Energy, 188, 819–829. doi:10.1016/j.renene.2022.02.023.

[40] Crook, J. A., Jones, L. A., Forster, P. M., & Crook, R. (2011). Climate change impacts on future photovoltaic and concentrated solar power energy output. Energy and Environmental Science, 4(9), 3101–3109. doi:10.1039/c1ee01495a.

[41] Gernaat, D. E. H. J., de Boer, H. S., Daioglou, V., Yalew, S. G., Müller, C., & van Vuuren, D. P. (2021). Climate change impacts on renewable energy supply. Nature Climate Change, 11(2), 119–125. doi:10.1038/s41558-020-00949-9.